AJNR

Diffusion Anisotropy in the Corpus Callosum

Neeraj B. Chepuri, Yi-Fen Yen, Jonathan H. Burdette, Hong Li, Dixon M. Moody and Joseph A. Maldjian

AJNR Am J Neuroradiol 2002, 23 (5) 803-808
http://www.ajnr.org/content/23/5/803

AJNR Am J Neuroradiol 23:803–808, May 2002

Diffusion Anisotropy in the Corpus Callosum

Neeraj B. Chepuri, Yi-Fen Yen, Jonathan H. Burdette, Hong Li, Dixon M. Moody, and Joseph A. Maldjian

BACKGROUND AND PURPOSE: **The corpus callosum is a heterogeneous white-matter tract that connects the cerebral hemispheres. The purpose of this investigation was to study its microstructural architecture in normal human adult brains by using diffusion tensor imaging (DTI).**

METHODS: **Two hundred consecutive patients referred for brain MR imaging underwent additional DTI with a high gradient field strength applied in six directions. Forty-two patients met the following inclusion criteria: 1) normal brain and 2) age greater than 18 years. Anisotropy maps were generated, and regions of interest were drawn around specified regions within the corpus callosum. Results were stratified by sex and age. In addition, available histologic specimens of the corpus callosum from cadaver brains were analyzed with conventional and specialized vascular staining.**

RESULTS: **Anisotropy values in the various regions of the corpus callosum differed significantly. Average values of the anisotropy index for the genu, body, and splenium of the corpus callosum were 0.400, 0.456, and 0.539, respectively. The differences between these values are statistically significant ($P < .01$). Increased anisotropy was present in posterior areas in both sexes and in all three age groups examined.**

CONCLUSION: **The results of this investigation show a statistically significant increase in anisotropy of the corpus callosum in its more posterior portions compared with its more anterior portions across sex and age groups. Although the microstructural etiology for this apparent increase in anisotropy is unclear, a number of possible mechanisms are presented.**

The corpus callosum is the major white-matter tract that crosses the interhemispheric fissure in the human brain. It consists of approximately 200 million interhemispheric fibers, most of which connect homologous regions of the cerebral cortex (1). Knowledge of its gross morphology and microscopic structure can be important in discriminating between health and disease of this important white-matter tract.

Numerous studies have been performed to examine the gross anatomic features of the corpus callosum, including its size and shape. These studies were performed with a combination of gross pathologic examination (2–4), CT (3), and MR imaging (1, 5–10). Fewer studies have been performed to analyze its light microscopic structure (2–4, 11).

With the advent of new MR imaging techniques that allow the rapid and rotationally invariant imaging of water diffusion in vivo, imaging of the diffusion characteristics of water within the human brain is now possible. Specifically, by calculating the diffusion tensor, both the magnitude and directionality of water diffusion in major white-matter tracts can be characterized (12–15). This knowledge leads to insights regarding the microscopic architecture of the white-matter tracts (13, 16). The purpose of this investigation was to determine the regional diffusion characteristics in the normal human adult corpus callosum. We hypothesized that no significant regional variation in diffusion anisotropy within the corpus callosum is present and that diffusion anisotropy is constant regardless of the age or sex of the patient.

Methods

Institutional review board approval was obtained to examine the usefulness of diffusion tensor imaging (DTI) in characterizing the human brain. Two hundred consecutive patients referred for brain MR imaging underwent additional DTI. Inclusion criteria for this study were the following: 1) an interpretation of a normal brain by two board-certified neuroradiologists and 2) age greater than 18 years. The application of the inclusion criteria resulted in the inclusion of 42 patients (12 male, 20 female; age range 18–80 years; mean age, 44.2 years, SD 13.8); these patients form the basis of this investigation.

Received October 23, 2001; accepted after revision February 11, 2002.

From the Department of Radiology, Wake Forest University School of Medicine, Bowman Gray Campus, Medical Center Boulevard, Winston-Salem, NC 27157.

Presented at the ASNR Annual Meeting in Boston, MA, 2001.

Address reprint requests to Neeraj B. Chepuri, MD, Wake Forest University School of Medicine, Radiology Department, Medical Center Boulevard, Winston-Salem, NC 27157.

DTI was performed by using single-shot spin-echo echo-planar readout on a clinical MR machine (LX Echospeed 1.5 T, GE Medical Systems, Milwaukee, WI) with a high gradient field strength (b = 3000 sec/mm^2). Gradients were applied in six directions, and the symmetry of the diffusion tensor was used to completely fill its 3 × 3 matrix. Images were obtained in the axial plane, with a maximum number of 21 sections to provide full brain coverage. The TR/TE was 3400/93.2, and the flip angle was 90°. The matrix size was 128 × 128, with a 24-cm field of view. The section thickness was 5 mm with a 1.5-mm intersection gap. Thus, the voxel dimensions were 1.875 × 1.875 × 5 mm. Eight excitations were used to increase the signal-to-noise ratio. The total imaging time for the additional DTI examination was 3 minutes 30 seconds.

Each of the 200 patients underwent routine brain MR imaging examinations; the findings were interpreted by board-certified neuroradiologists (J.H.B., D.M.M., J.A.M., N.B.C.). Of the 42 normal patients, clinical indications for brain imaging included headache in 26 patients, mental status change in 21 patients, nausea and/or vomiting in 18, syncope in 13, dizziness in nine, and visual changes in four. The complete brain MR imaging examination included sagittal and axial spin-echo T1-weighted imaging (600/15), axial fast spin-echo T2-weighted imaging (3000/100), coronal fluid-attenuation inversion recovery (FLAIR) imaging (TR/effective TE/TI, 8000/112/2700), and axial diffusion-weighted imaging (10,000/96.8, one excitation, b = 1000 s/mm^2). Thirty-two of the 42 examinations included an intravenous injection of gadolinium-based contrast agent (0.1 mmol/kg Magnevist (gadopentetate dimeglumine); Berlex Laboratories, Wayne, NJ) followed by axial and coronal spin-echo T1-weighted imaging (600/15). DTI was always performed prior to the administration of the contrast agent. The source data from the DTI examination were available at the time of interpretation, but calculated anisotropy maps and directionality maps were not available at that time.

Brain MR imaging findings were interpreted as normal when they were within a normal range, given the patient's age. Thus, patients with cerebral atrophy were excluded from the study only when the amount of atrophy was considered abnormal for their age. Similarly, patients with focal white-matter hyperintensities were excluded from this investigation only if the amount of disease was considered to be abnormal for the patient's age. These determinations were based on the clinical experience of the neuroradiologists, rather than on any physical measurement. Neurocognitive assessment was not performed in any patient.

The imaging data for the 42 patients who satisfied the inclusion criteria were transferred off-line to a Unix-based Sun workstation and analyzed with locally developed software that performed the following functions: 1) Data from the DTI sequence were diagonalized to create the full diffusion tensor for each voxel (see the Appendix for a discussion of the process of diagonalization). 2) Anisotropy maps were generated by calculating an anisotropy index within each voxel. The anisotropy index was calculated by using the volume-ratio method discussed in reference 13 and in the Appendix. 3) Regions of interest (ROIs) were drawn directly on to the anisotropy maps, with ROIs corresponding to the areas of maximum anisotropy identified in the genu, body, and splenium of the corpus callosum. The ROIs were manually drawn onto the anisotropy maps by using the image obtained with a b value of 0 in the same echo-planar sequence used to provide anatomic landmarks. Regions of maximum anisotropy were included within the ROIs. For this reason, the ROIs did vary in size. However, obtained anisotropy values were weighted by ROI size. Typical ROI sizes were 4 cm^3 in the genu, 12 cm^3 in the body, and 8 cm^3 in the splenium. This process resulted in a list of anisotropy indices for each location in each patient.

The anisotropy index values were entered into a database by region of the corpus callosum (ie, genu, body, splenium). Statistical analysis was performed between these regions by using a two-tailed Student *t* test for paired data. This analysis was first performed across all patients, then sex, and finally with stratified age groups (ie, 18–30, 31–50, and 51–80 years).

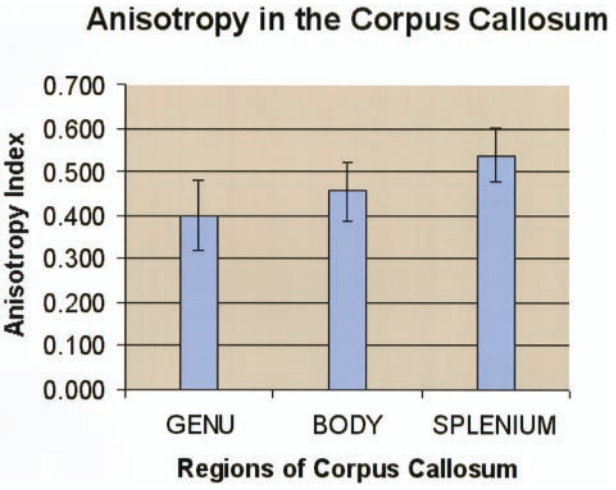

FIG 1. Graphical representation of anisotropy data obtained from different regions of the corpus callosum in all 42 patients. Anisotropy data were calculated by using the volume-ratio method as discussed in the Appendix. A value of 0 represents perfect isotropy; 1 represents perfect anisotropy.

In addition, available thick celloidin sections of the corpus callosum (from cadaver brains) with specialized vascular staining (alkaline phosphatase), cut in axial and sagittal planes, were qualitatively examined for features that might explain the observed diffusion anisotropy findings. Because of the limited histologic material available, quantitative analysis was not performed, and analyses by callosal region (ie, genu, body, splenium) could not be performed.

Results

Figure 1 summarizes mean anisotropy data obtained in the genu, body, and splenium of the corpus callosum in all 42 patients. The value of the anisotropy index used in this investigation (Appendix) ranged from 0 to 1, where 0 signified perfect isotropy, and 1 signified perfect anisotropy. Across all patients, the average value of the anisotropy index in the splenium was 0.539. The corresponding values in the body and genu were 0.456 and 0.400, respectively. Thus, anisotropy was highest in the splenium, followed by the body, and then the genu. All of these differences were statistically significant when analyzed with a two-tailed Student *t* test for paired data ($P < .01$).

Similar results were obtained when the patients were separated by sex. Average anisotropy values for the 30 women in the investigation were 0.411, 0.453, and 0.547 in the were genu, body, and splenium of the corpus callosum, respectively. Average anisotropy values for the 12 men in the investigation were 0.373, 0.466, and 0.519 in the genu, body, and splenium of the corpus callosum, respectively. Intracallosal value differences were all statistically significant when analyzed with a two-tailed Student *t* test for paired data ($P < .01$).

Stratification by patient age also yielded similar results. Average anisotropy values for the eight patients in the 18–30-year age group were 0.392, 0.449,

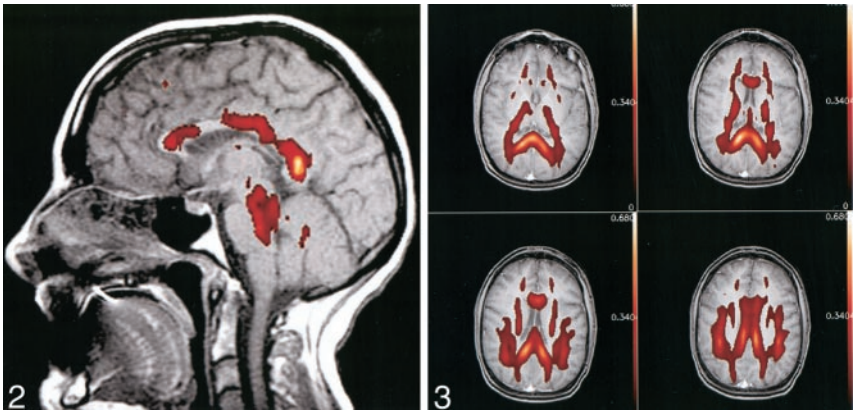

FIG 2. Typical appearance of anisotropy in healthy human adult brain. Anisotropy maps obtained with the volume-ratio method are represented by *color overlay* on a gray-scale sagittal spin-echo T1-weighted image. Note the increased anisotropy of the posterior aspect of the corpus callosum compared with that of the anterior portion.

FIG 3. Typical appearance of anisotropy in healthy human adult brain. The same anisotropy maps from Figure 2 were overlaid on four axial spin-echo T1-weighted images through the corpus callosum.

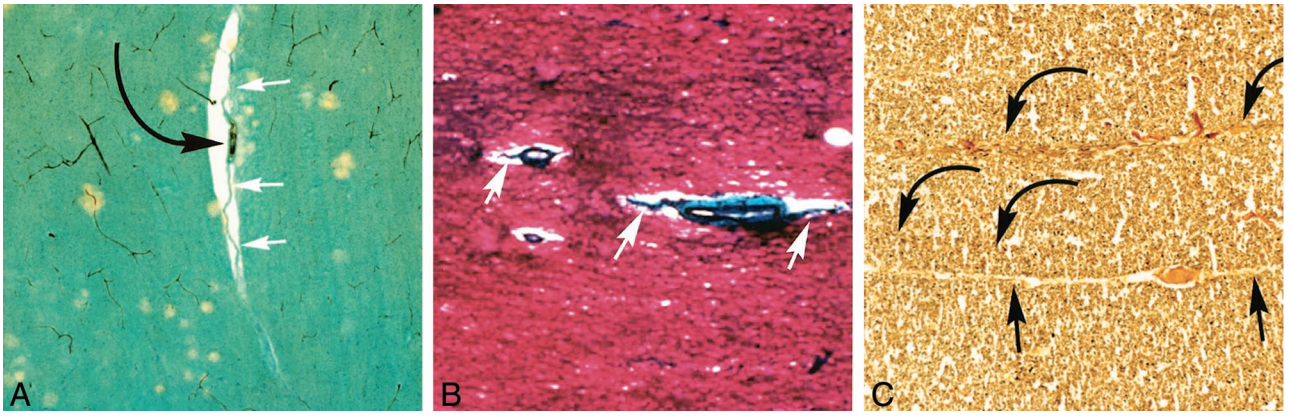

FIG 4. Histologic findings in cadaver corpora callosa

A, Perivascular fibrous alae on a sagittal celloidin 100-μm-thick section through the corpus callosum (alkaline phosphatase stain, cresyl violet acetate and light green counterstain). A large arteriole (*black arrow*) is obliquely sectioned, and the extent of the collagenous perivascular ala (*white arrows*) is seen in an artifactual gap in the tissue.

B, Axial celloidin 100-μm-thick section through the corpus callosum (alkaline phosphatase stain, trichrome counterstain). Collagenous (*green*) sheets (*arrows*) are contiguous with and extend laterally away from penetrating callosal arterioles. These alae descend through the corpus callosum in a curtain-like fashion. Note that the axons horizontally oriented in this section.

C, Sagittal paraffin 10-μm-thick section through the corpus callosum (Bielschowsky stain). Axons are stained black, and most are cut in cross-section and appear as black dots (as expected). Two small bundles of obliquely oriented axons (*curved arrows*) are depicted. Obliquely cut vessels and associated fibrous ala are seen in a tissue cleft (*straight arrows*).

and 0.545 in the genu, body, and splenium of the corpus callosum respectively. Average anisotropy values for the 21 patients in the 31–50-year age group were 0.406, 0.457, and 0.546 in the genu, body, and splenium of the corpus callosum, respectively. Average anisotropy values for the eight patients in the 51–80-year age group were 0.394, 0.459, and 0.526 in the genu, body, and splenium of the corpus callosum, respectively. Intracallosal value differences were all statistically significant when analyzed with a two-tailed Student *t* test for paired data ($P < .01$).

Figures 2 and 3 demonstrate typical findings. Figure 2 is a color representation of an anisotropy index map overlaid on a midsagittal spin-echo T1-weighted image through the corpus callosum in a single patient. Figure 3 shows the same anisotropy map data in the axial plane, overlaid on spin-echo T1-weighted images through the corpus callosum (also in a single patient). Both figures show that anisotropy values in the posterior portions of the corpus callosum were greater than those in the anterior portions.

Figure 4 shows images from the histologic sections from the cadaver brains that were available to us. The histologic sections confirmed that most axonal fibers were directed horizontally. Small bundles of obliquely oriented axons were also present. Vertical sheetlike bands of collagenous tissue extended for variable distances (side to side) from the major penetrating arterioles. Because of the limited amount of histologic tissue available, only qualitative analyses were performed, and the various regions of the corpus callosum could not be compared.

Discussion

DTI of water molecules within the human brain may provide valuable, previously unknown clues to the microstructure of white-matter tracts (12–14, 16). The presence of diffusion anisotropy in the corpus callosum is expected (15, 16). However, the presence of statistically significant regional differences in anisotropy within the corpus callosum nullifies our hypothesis (see Introduction) and raises important questions regarding its microstructure. The explanation for this finding may lie in the regional differences of the microscopic structure of the corpus callosum that are due

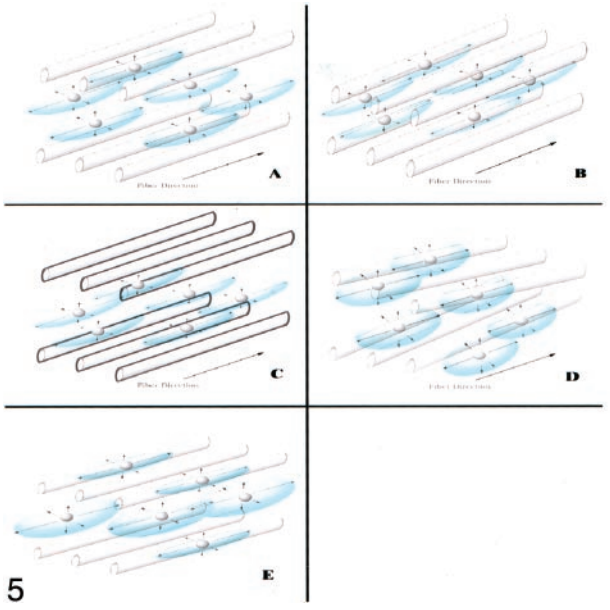

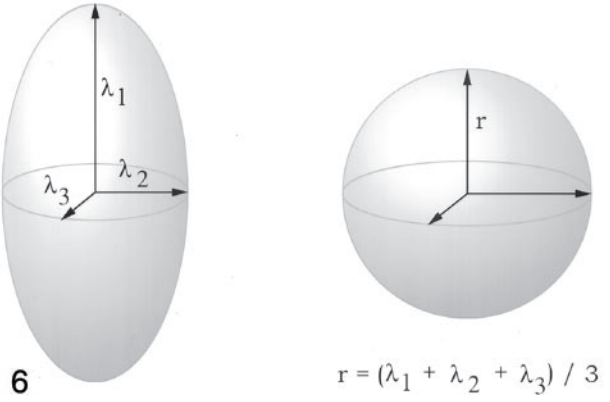

FIG 5. Schematic representation of diffusion anisotropy in brain white matter. Obliquely oriented *cylinders* represent axonal fibers and myelin sheaths, and small *spheres* represent water molecules. When the randomly chosen direction of diffusion is transverse to the fiber direction, the path of diffusion is blocked by hydrophobic myelin sheaths. When the randomly chosen direction of diffusion is parallel to the fiber direction, there are no barriers to free diffusion. Thus, the water molecules demonstrate a preference for diffusion along the direction of the fiber tract (12, 13, 16) (*A*). Schematic representations illustrate the situations in which axons are more tightly packed (*B*), the myelin sheaths are thicker (*C*), obliquely oriented axons are present (*D*), and the axonal diameter is reduced (*E*).

FIG 6. Schematic representation of the ellipsoid that describes the mean diffusion of a water molecule at the center of a voxel in all directions. The eigenvalues of the diagonalized diffusion tensor (λ_1, λ_2, λ_3) are the axes of this ellipsoid. Also represented is a sphere with a radius that is the average value of the three axes of the corresponding ellipsoid. The volume ratio used is the ratio of the volume of the ellipsoid to the volume of the sphere, as discussed in the Appendix and in reference 13. The anisotropy index used in this investigation was as follows: 1 − volume ratio.

to regional variations in normal development or regional variations in age-related effects (1, 12, 17, 18). This finding may be an important clue regarding the organization of the corpus callosum, and it may help to explain the behavior of the corpus callosum in diseased states (eg, when it is affected by vasogenic edema or demyelinating disease) (3, 11, 14, 19). Importantly, however, the current investigation does not provide proof of a histologic substrate for our findings. Rather, we are merely advancing plausible explanations for our findings.

Microscopic Factors Affecting Diffusion Anisotropy

Our limited evaluation of histologic material from cadaver corpora callosa (Fig 4) did not provide us with a definitive histologic substrate to explain our findings. Further analysis of callosal specimens may provide insight in the future. However, we do recognize that a number of microscopic factors may explain our findings (6, 7, 14, 16, 17). These factors are listed here and graphically illustrated in Figure 5, in which the axonal projections and myelin sheaths of nerve cells are represented by long, thin, parallel cylinders. The random motion of intra- and extracellular water can occur in any direction. In this scenario, however, water movement transverse to the direction of fiber orientation is restricted by the hydrophobic myelin sheaths. There is no barrier to motion in the direction of the fiber tract. Thus, water diffuses preferentially in the direction of the fiber tracts, and anisotropy is greater than 0. Factors that may increase the anisotropy present in white matter include the following: 1) tighter packing of axons, 2) less permeable (or thicker) myelin sheaths, 3) fewer obliquely oriented axons, 4) altered radius of individual axons, and 5) the presence of structures other than myelin sheaths within the corpus callosum that restrict water diffusion (11).

Of note, the presence of obliquely oriented fibers in the corpus callosum was observed in our investigation and reported in the literature (11). The body of the corpus callosum is likely to contain the greatest number of obliquely oriented fibers because it primarily transmits the commissural fibers that connect heterologous regions of the cerebral cortex (2, 4). However, to our knowledge, the increased presence of obliquely oriented fibers in the body compared with the remainder of the corpus callosum has not been demonstrated. Also, we could not make this determination on the basis of our limited histologic material.

Another factor that may produce diffusion anisotropy is the presence (or absence) of structures other than the axonal fibers. These include the collagenous perivascular fibrous alae that were demonstrated in this investigation (Fig 4) and in previous reports in the literature that involved conventional and histochemical staining with light microscopy with thick

celloidin sections (11). These structures are difficult to see on the usual thin paraffin sections, particularly when the plane of the autopsy section is coronal or coronal oblique. These structures are winglike extensions of the fibrous adventitia of penetrating callosal arterioles (Fig 4). They form a sheet of collagen that is 10–15 μm in thickness with a span of as long as 5 mm; this sheet is arranged in the coronal or oblique coronal plane, depending on the curvature of the corpus callosum. When viewing this in the axial plane, we observed that that these collagenous perivascular alae could present an incomplete, staggered barrier to the anteroposterior flow of extracellular fluid (Fig 4). At this time, the presence of regional differences in the corpus callosum of the collagenous perivascular alae is unknown.

Differential Regional Development and Aging of the Corpus Callosum

Differences in the normal development or aging process of the corpus callosum may possibly explain our findings. This possibility is supported by the observation of intracallosal regional differences related to both development (8) and aging (9, 10).

Regional differences in the development of the corpus callosum during the 1st year of life have been described, with growth spurts for various regions of the corpus callosum occurring at different times (8). At birth, the splenium is intermediate in size compared with the genu and body of the corpus callosum. The first identifiable change occurs during the 2nd and 3rd months after birth, when the genu focally enlarges. The next identifiable change occurs in the splenium, which slowly enlarges during the first 4 months until a rapid growth spurt occurs during the 5th and 6th postnatal months, which results in its bulbous appearance. The body of the corpus callosum slowly enlarges during the 1st year of life, without any identifiable growth spurts (8). In addition, pathologic studies have shown that the fibers crossing through different regions of the corpus callosum serve different functions; varying fractions of these fibers connect heterologous areas of cortex (2, 4, 8).

Numerous previous studies (9, 10) have also examined the effects of aging on the corpus callosum. These studies show a generalized decrease in the thickness of the corpus callosum with advancing age. However, the only statistically significant regional change with aging occurs in the body of the corpus callosum, which decreases in thickness and cross-sectional area. In addition, certain degenerative diseases associated with aging (eg, Alzheimer disease) do have a regional preference in causing atrophy of the corpus callosum. In the specific case of Alzheimer disease, the thickness of the genu decreases to a greater extent than the remainder of the corpus callosum, when patients are compared with age-matched control subjects (1).

Issues Related to This Investigation

Statistical analysis of 42 normal adult human brains allows enough power to determine significant differences between the means with a high degree of certainty. However, despite the interpretation of normal brain by board-certified neuroradiologists in these 42 patients, these cases are drawn from a pool of 200 patients referred for MR imaging of the brain for a clinical reason. Therefore, although these brain MR findings were normal, they may not be truly representative of the community population. In light of the demonstration of occult white-matter pathology in many neurologic conditions, judging the degree to which these data reflect the situation of the corpus callosum in healthy control subjects is difficult. However, the demographic stratification we performed did show that the effect of increased anisotropy in posterior areas within the corpus callosum was present regardless of sex or age; this finding suggested, but did not prove, that this observation may represent the case in healthy control subjects as well.

We obtained the anisotropy images in the axial plane rather than in the sagittal plane, with multiple sections through the corpus callosum. We believe that this approach results in more representative images of the entire corpus callosum than the acquisition of a single midsagittal image. Although partial-volume effects may have been included in our measurements, we do not believe that partial-volume artifact played a significant role in our measurements, for the following reasons: 1) When ROIs were drawn on the anisotropy maps, only the central (most anisotropic) portions of the corpus callosum were included. 2) If partial-volume effects were causing regional differences in measured anisotropy, we would have expected the standard deviations of measured data in the various regions to be different as well. As Figure 1 shows, the standard deviations among the regions were similar.

Finally, the amount of histologic corpus callosum material that was available to us was limited. Thus, only qualitative observations could be made, and histologic analysis of callosal subregions was not possible. This may be the subject of future investigation.

Conclusion

Using DTI, we have found significant differences in diffusion anisotropy within the various portions of the corpus callosum in a cohort of 42 healthy adult patients. Specifically, we showed that anisotropy in the posterior portions of the corpus callosum was significantly increased in comparison with its more anterior portions (anisotropy value for splenium $>$ body value $>$ genu value) across sex and age groups. On the basis of a review of the literature and the histologic findings from our corpus callosum sections, we propose that these anisotropic variances in the corpus callosum may be due to a combination of the following physical and geometric factors: 1) tighter packing of axons, 2) less permeable myelin sheaths, 3) fewer obliquely oriented axons, 4) altered radius of individ-

ual axons, and 5) the presence (or absence) of collagenous perivascular alae. Further investigation of the normal human corpus callosum with light and/or electron microscopy may provide more information to account for our findings.

Appendix: Calculation of Anisotropy Index

Anisotropy values in this investigation are calculated as described by Pierpaoli and Basser (13) by using the intravoxel volume ratio method. The initially measured data reflect the diffusion of water in six directions. In addition to the three mutually perpendicular directions of water diffusion (d_{xx}, d_{yy}, d_{zz}), cross-terms were obtained (d_{xy}, d_{yz}, d_{xz}). These can be represented in a 3×3 matrix, or diffusion tensor, by using the symmetry of the diffusion tensor to fill in the entire matrix, as follows:

$$\begin{matrix} d_{xx} & d_{xy} & d_{xz} \\ d_{xy} & d_{yy} & d_{yz} \\ d_{xz} & d_{yz} & d_{zz}. \end{matrix}$$

The 3×3 matrix is then diagonalized, yielding a 3×3 matrix with nondiagonal terms that are 0. The diagonalization process yields a 3×3 matrix multiplied by another 3×3 matrix θ that represents the directionality of the tensor, as follows:

$$\begin{matrix} \lambda_1 & 0 & 0 \\ 0 & \lambda_2 & 0 \\ 0 & 0 & \lambda_3. \end{matrix}$$

The three remaining diagonal terms are called λ_1, λ_2, and λ_3. These three eigenvalues represent the magnitude of the three orthogonal axes of the ellipsoid that describes the mean diffusion of a water molecule at the center of the voxel in all directions (Fig 6).

The volume-ratio parameter described by Pierpaoli and Basser (13) is the ratio of the volume of the ellipsoid ($V_{ellipsoid}$) described by the axes λ_1, λ_2, and λ_3 divided by the volume of the sphere (V_{sphere}) with a radius equal to the average of λ_1, λ_2, and λ_3, as follows:

1) $$\text{Volume Ratio} = V_{ellipsoid}/V_{sphere}.$$

$V_{ellipsoid}$ is calculated as follows:

2) $$V_{ellipsoid} = (4/3)\pi(\lambda_1 \lambda_2 \lambda_3).$$

V_{sphere} is calculated as follows:

3) $$V_{sphere} = (4/3)\pi r^3.$$

Because $r = (\lambda_1 + \lambda_2 + \lambda_3)/3$, or the average of the three axes of the ellipsoid, the volume of the sphere is determined as follows:

4) $$V_{sphere} = (4/3)\pi[(\lambda_1 + \lambda_2 + \lambda_3)/3]^3.$$

By substituting Equations 2 and 4 into equation 1 and by eliminating the common terms, we obtain the following formula for the volume ratio:

5) $$\text{Volume Ratio} = 27(\lambda_1 \lambda_2 \lambda_3)/(\lambda_1 + \lambda_2 + \lambda_3).$$

As anisotropy increases (ie, as the ellipsoid becomes more needlelike), λ_3 approaches 0. Therefore, the numerator of the volume ratio approaches 0. As anisotropy decreases, the volume of the ellipsoid approaches the volume of the sphere, and the volume ratio approaches 1. This effect is the opposite that of the desired anisotropy index, which increased with increasing anisotropy. Thus, the anisotropy index is defined as follows:

6) $$\text{Anisotropy Index} = 1 - (\text{Volume Ratio}).$$

References

1. Biegon A, Eberling JL, Richardson BC, et al. **Human corpus callosum in aging and Alzheimer's disease: a magnetic resonance imaging study.** *Neurobiol Aging* 1994;15:393–397
2. Cumming WJ. **An anatomical review of the corpus callosum.** *Cortex* 1970;6:1–18
3. Cowley AR. **Dyke award: influence of fiber tracts on the CT appearance of cerebral edema—anatomic-pathologic correlation.** *AJNR Am J Neuroradiol* 1983;4:915–925
4. Rakic P, Yakovlev PI. **Development of the corpus callosum and cavum septi in man.** *J Comp Neurol* 1968;132:45–72
5. Parashos IA, Wilkinson WE, Coffey CE. **Magnetic resonance imaging of the corpus callosum: predictors of size in normal adults.** *J Neuropsychiatry Clin Neurosci* 1995;7:35–41
6. Doraiswamy PM, Figiel GS, Husain MM, et al. **Aging of the human corpus callosum: magnetic resonance imaging in normal volunteers.** *J Neuropsychiatry Clin Neurosci* 1991;3:392–397
7. Rajapakse JC, Giedd JN, Rumsey JM, et al. **Regional MRI measurements of the corpus callosum: a methodological and developmental study.** *Brain Dev* 1996;18:379–388
8. Barkovich AJ, Kjos BO. **Normal postnatal development of the corpus callosum as demonstrated by MR imaging.** *AJNR Am J Neuroradiol* 1988;9:487–491
9. Ferrario VF, Sforza C, Serrao G, Frattini T, Del Favero C. **Shape of the human corpus callosum. Elliptic Fourier analysis on midsagittal magnetic resonance scans.** *Invest Radiol* 1994;29:677–681
10. Hayakawa K, Konishi Y, Matsuda T, et al. **Development and aging of brain midline structures: assessment with MR imaging.** *Radiology* 1989;172:171–177
11. Moody DM, Bell MA, Challa VR. **The corpus callosum, a unique white-matter tract: anatomic features that may explain sparing in Binswanger disease and resistance to flow of fluid masses.** *AJNR Am J Neuroradiol* 1988;9:1051–1059
12. Melhem ER, Itoh R, Jones L, Barker PB. **Diffusion tensor MR imaging of the brain: effect of diffusion weighting on trace and anisotropy measurements.** *AJNR Am J Neuroradiol* 2000;21:1813–1820
13. Pierpaoli C, Basser PJ. **Toward a quantitative assessment of diffusion anisotropy.** *Magn Reson Med* 1996;36:893–906
14. Wimberger DM, Roberts TP, Barkovich AJ, et al. **Identification of "premyelination" by diffusion-weighted MRI.** *J Comput Assist Tomogr* 1995;19:28–33
15. Assaf Y, Ben-Bashat D, Chapman J, et al. **High b-value q-space analyzed diffusion-weighted MRI: Application to multiple sclerosis.** *Magn Reson Med* 2002;47:115–126
16. Basser PJ, Pierpaoli C. **Microstructural and physiological features of tissues elucidated by quantitative-diffusion-tensor MRI.** *J Magn Reson B* 1996;111:209–219
17. Guo AC, Jewells VL, Provenzale JM. **Analysis of normal-appearing white matter in multiple sclerosis: comparison of diffusion tensor MR imaging and magnetization transfer imaging.** *AJNR Am J Neuroradiol* 2001;22:1893–1900
18. Bozzali M, Franceschi M, Falini A, et al. **Quantification of tissue damage in AD using diffusion tensor and magnetization transfer MRI.** *Neurology* 2001;57:1135–1137
19. O'Sullivan M, Summers PE, Jones DK, et al. **Normal-appearing white matter in ischemic leukoaraiosis: a diffusion tensor MRI study.** *Neurology* 2001;57:2307–2310